Available online at www.sciencedirect.com
SCIENCE DIRECT®
International Journal of Heat and Mass Transfer 48 (2005) 4569–4578
International Journal of HEAT and MASS TRANSFER
www.elsevier.com/locate/ijhmt

# DNS of fully developed turbulent heat transfer of a viscoelastic drag-reducing flow

Bo Yu [a], Yasuo Kawaguchi [b,*]

[a] Department of Oil and Gas Storage and Transportation Engineering, China University of Petroleum, Beijing 102249, People's Republic of China
[b] Department of Mechanical Engineering, Faculty of Science and Technology, Tokyo University of Science, 2641 Yamazaki, Noda, Chiba 278-8510, Japan

Received 27 August 2003; received in revised form 16 February 2005

**Abstract**

A direct numerical simulation (DNS) of turbulent heat transfer in a channel flow with a Giesekus model was carried out to investigate turbulent heat transfer mechanism of a viscoelastic drag-reducing flow by additives. The configuration was a fully-developed turbulent channel flow with uniform heat flux imposed on both the walls. The temperature was considered as a passive scalar with the effect of buoyancy force neglected. The Reynolds number based on the friction velocity and half the channel height was 150. Statistical quantities such as root-mean-square temperature fluctuations, turbulent heat fluxes and turbulent Prandtl number were obtained and compared with those of a Newtonian fluid flow. Budget terms of the temperature variance and turbulent heat fluxes were also presented.


## 1. Introduction

Although Toms' effect, which is the reduction of turbulent friction drag with the addition of a very small amount of long-chain polymer into pipe liquid flow, was discovered in 1948 [1] and many experiments have been performed to study this phenomenon in the decades since then, the mechanism of drag-reducing turbulent flow by additives has not been satisfactorily clarified. This is partly due to the limitation of present experimental facilities, with which it is extremely difficult to measure various instantaneous quantities such as velocity and pressure in the vicinity of the walls with sufficient accuracy. DNS is an alternative tool to study the physics of turbulence and can identify instantaneous turbulent flow structures for thorough analysis. DNS has recently been used to study drag-reducing flow by additives [2–11], and it was found that a viscoelastic model can reproduce most of the experimental observations such as wider buffer layer, reduction of Reynolds shear stress and larger spacing between low-speed streaks. Experiments show that due to the dramatic suppression of turbulence, the heat transfer coefficients in drag-reducing flows with surfactant additives are also reduced [12,13]. A better understanding of the mechanism of turbulent heat transfer in drag-reducing flow by additives is interesting and important from both scientific and engineering perspectives. To the author's knowledge, no numerical simulation of the turbulent heat transfer of drag-reducing flow has been carried out. In this paper

* Corresponding author. Fax: +81 4 7123 9814.
*E-mail address:* yasuo@rs.noda.tus.ac.jp (Y. Kawaguchi).

0017-9310/$ - see front matter © 2005 Published by Elsevier Ltd.
doi:10.1016/j.ijheatmasstransfer.2005.04.032

**Nomenclature**

| | |
|---|---|
| $c$ | conformation tensor |
| $C_f$ | friction factor $= 2\tau_w/\rho U_b^2$ |
| $c_P$ | specific heat at constant pressure (J/(kg K)) |
| $E_{tt}(k_z)$ | one-dimensional energy spectra of temperature fluctuations $\frac{2}{NzAz^*}\left\|\sum_{n=1}^{Nz}\theta'^+(n\Delta z^*)\, e^{-i2\pi kn/Nz}\Delta z^*\right\|^2$, $k = 1,2,\ldots,Nz/2$ |
| $h$ | half height of the channel (m) |
| $h^*$ | heat transfer coefficient (W/(m$^2$ K)) |
| $k$ | thermal conductivity (W/(m K)) |
| $k_z$ | wave number for spanwise direction $= 2\pi k/(Nz\Delta z^*)$, $k = 1,2,\ldots,Nz/2$ |
| $k_\theta$ | temperature variance $= \overline{\theta'^{+2}}/2$ |
| $Nu$ | Nusselt number $= 2h^*h/k$ |
| $p$ | pressure (Pa) |
| $Pr$ | molecular Prandtl number |
| $Pr_t$ | turbulent Prandtl number $= \nu_t/a_t$ |
| $q_w$ | wall heat flux (W/m$^2$) |
| $q_{total}$ | total heat flux (W/m$^2$) |
| $Re_b$ | Reynolds number $= 2\rho U_b h/\eta_s$ |
| $Re_\tau$ | Reynolds number $= \rho u_\tau h/\eta_s$ |
| $t$ | time (s) |
| $t$ | nondimensional time |
| $T$ | temperature (°C, K) |
| $T_b$ | bulk mean temperature (°C) |
| $T_\tau$ | friction temperature $= q_w/\rho c_P u_\tau$ |
| $u$ | velocity (m/s) |
| $U$ | mean streamwise velocity (m/s) |
| $U_c$ | mean centerline velocity (m/s) |
| $U_b$ | mean bulk velocity (m/s) |
| $u_\tau$ | friction velocity $= \sqrt{\tau_w/\rho}$ (m/s) |
| $We_\tau$ | Weissenberg number $= \rho\lambda u_\tau^2/\eta_s$ |
| $x_1, x$ | streamwise direction (m) |
| $x_2, y$ | wall-normal direction (m) |
| $x_3, z$ | spanwise direction (m) |

*Greek symbols*

| | |
|---|---|
| $\alpha$ | mobility factor |
| $\alpha_t$ | eddy-diffusivity for heat $= -\overline{v'^+\theta'^+}/\mathrm{d}\Theta^+/\mathrm{d}y^+$ |
| $\beta$ | ratio $= \eta_a/\eta_s$ |
| $\eta_a$ | dynamic shear viscosity of additive contribution (Pa s) |
| $\eta_s$ | dynamic shear viscosity of solvent contribution (Pa s) |
| $\eta_0$ | shear viscosity of the viscoelastic solution at zero-shear rate $= \eta_a + \eta_s$ (Pa s) |
| $\lambda$ | relaxation time (s) |
| $\theta$ | local temperature difference $= \langle T_w\rangle - T$ (°C) |
| $\Theta$ | par mean local temperature (°C) |
| $\Theta_b$ | mixed mean temperature (°C) |
| $\nu_t$ | eddy-diffusivity for momentum $= -\overline{u'^+v'^+}/\mathrm{d}U^+/\mathrm{d}y^+$ |
| $\rho$ | density (kg/m$^3$) |
| $\tau_w$ | statistically averaged wall shear stress (kg/(m s$^2$)) |

*Superscripts and subscripts*

| | |
|---|---|
| $(\,)'$ | fluctuating component |
| $(\,)^+$ | normalized by $u_\tau$, $\rho$, $\eta_s$ and $T_\tau$ |
| $(\,)^*$ | nondimensional coordinate |
| $(\,)_{rms}$ | root-mean-square fluctuations |
| $\langle\,\rangle$ | enable average over the spanwise direction and time |

we first attempt to perform a DNS study on the turbulent heat transfer of the drag-reducing flow in a channel with uniform heat flux imposed on the walls at a low Reynolds number $Re_\tau = 150$. We then compare the results with those of Newtonian flow.

## 2. Fundamental equations and computational method

The flow to be studied was a fully-developed channel flow as shown in Fig. 1, in which $x$, $y$ and $z$ are the streamwise, wall-normal and spanwise directions, respectively, and the corresponding velocity components are $u$, $v$ and $w$. The top and bottom walls were heated by a uniform heat flux $q_w$. In this study we employed a viscoelastic model—Giesekus constitutive equation to calculate the extra stress due to additives. The dimensionless governing equations for the fully-developed turbulent isoflux channel flow can be written as

$$\frac{\partial u_i^+}{\partial x_i^*} = 0 \tag{1}$$

$$\frac{\partial u_i^+}{\partial t^*} + u_j^+\frac{\partial u_i^+}{\partial x_j^*} = -\frac{\partial p^+}{\partial x_i^*} + \frac{1}{Re_\tau}\frac{\partial}{\partial x_j^*}\left(\frac{\partial u_i^+}{\partial x_j^*}\right) + \frac{\beta}{We_\tau}\frac{\partial c_{ij}^+}{\partial x_j^*} + \delta_{1i} \tag{2}$$

$$\frac{\partial \theta^+}{\partial t^*} + u_j^+\frac{\partial \theta^+}{\partial x_j^*} = \frac{2u^+}{\int_{-1}^{1} U^+\,\mathrm{d}y} + \frac{1}{Re_\tau Pr}\frac{\partial}{\partial x_j^*}\left(\frac{\partial \theta^+}{\partial x_j^*}\right) \tag{3}$$

$$\frac{\partial c_{ij}^+}{\partial t^*} + \frac{\partial u_m^+ c_{ij}^+}{\partial x_m^*} - \frac{\partial u_i^+}{\partial x_m^*}c_{mj}^+ - \frac{\partial u_j^+}{\partial x_m^*}c_{mi}^+ + \frac{Re_\tau}{We_\tau}[c_{ij}^+ - \delta_{ij} + \alpha(c_{im}^+ - \delta_{im})(c_{mj}^+ - \delta_{mj})] = 0 \tag{4}$$

In the above equations, $c_{ij}^+$ is the conformation component due to the elasticity of the solution, and $\beta$ ($\beta = \eta_a/\eta_s$) is the ratio between the additive contribution $\eta_a$ and solvent contribution $\eta_s$ to the zero-shear rate

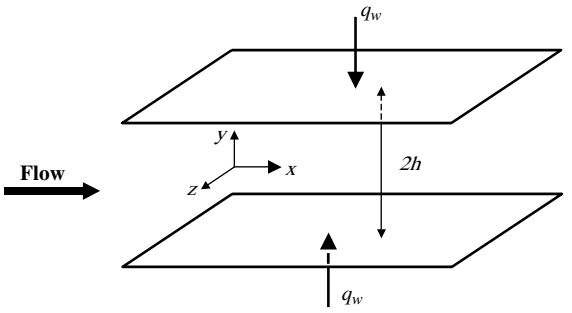


Fig. 1. Computational domain.

viscosity $\eta_0$ ($\eta_0 = \eta_a + \eta_s$). The Reynolds number and Weissenberg number are defined as: $Re_\tau = \rho u_\tau h/\eta_s$ and $We_\tau = \rho\lambda u_\tau^2/\eta_s$, where $\rho$, $\lambda$, $u_\tau$ and $h$ are the fluid density, relaxation time, friction velocity and half the channel height, respectively. Note that the Reynolds number and Weissenberg number are based on the viscosity of solvent. By setting $\beta = 0$, the Navier–Stokes equation for a Newtonian fluid is obtained. A calculation was carried out for the Newtonian fluid for comparison. Table 1 shows the dimensionless computational parameters.

It is known that the smallest scale in temperature fluctuation decreases with the increase of Prandtl number inversely proportional to $Pr^{1/2}$ [15]. At a first step, the change of the turbulent characteristics by the viscoelasticity was investigated. In order overcome thermal resolution barrier by relatively large Prandtl number of water, we change the Prandtl number to 0.71. Our next step is to use fine meshes for the calculation of high Prandtl number turbulence flows.

The periodic boundary conditions were imposed in both the streamwise ($x$-) and spanwise ($z$-) direction, while nonslip and isoflux boundary conditions were adopted for the top and bottom walls. Unlike velocity and temperature components, the conformation components at the walls evolve in time and their values were determined from Eq. (3) by setting the velocity components at the walls zero. An instantaneous velocity field of Newtonian fluid at Reynolds number $Re_\tau = 150$ from our previous work [10] was adopted as the initial velocity field. The initial fields for pressure and conformation tensor were simply set as a zero field.

A fractional step method was employed for the computation algorithm. The Adams–Bashforth scheme was used for the time advancement except that the implicit method was adopted for the time advancement of the pressure. For spatial discretization, a second-order finite difference scheme was employed. In the preceding DNSs, spectral method was preferred owing to its higher-numerical accuracy. But finite difference scheme is easier to be applied to complex geometry and complicated boundary conditions. The studies [2,16,17] show that the resolution of finite difference schemes is comparable to that of spectral method at least for lower-order statistical quantities as the grid size is fine enough to sustain turbulence. This does not mean that the finite difference scheme is as accurate as spectral method. But it has been proven that as fine as the mesh required by DNS is satisfied, the solutions of the two schemes are comparable. On the other hand, unlike Newtonian fluid flow, DNS of viscoelastic flow is prone to break down due to the hyperbolic nature of the constitutive equation. To enhance numerical stability, artificial diffusion terms were introduced in the constitutive equations by using spectral method [4,5,7]. It is well known that for the DNS calculation significant artificial viscosity should be avoided [16] and it is necessary to analyze the effect of artificial diffusion (AD) term on the solution accuracy. Our previous analysis shows that the error introduced by the AD term is much larger than the discretization error of the spectral method and actually the AD spectral method is a lower-order scheme [9]. For finite difference scheme we employed a high-resolution scheme, MINMOD to descretizte the convective term in the constitutive equation and by using this scheme no artificial term was required. It was found that MINMOD scheme is not only more accurate but also more stable than artificial diffusion spectral method [9]. For this reason, we chose the high-resolution finite difference scheme for spatial discretization in the present study. To avoid zigzag pressure field, staggered grid was employed in which pressure and conformation components were stored at the cell center while velocity components locate at the cell faces.

A larger computational domain was used for the drag-reducing flow because coherent structures in the turbulent flow of the drag-reducing flow are much more elongated due to the relaxation time, and a coarser mesh was adopted for the drag-reducing flow because of larger eddy sizes in the drag-reducing flow [9–11].

The friction factor and Nusselt number are evaluated by

$$C_f = \frac{\tau_w}{\rho U_b^2/2} = \frac{2}{U_b^{+2}} \tag{5}$$

Table 1
Computational parameters

| | $Re_\tau$ | $We_\tau$ | $\beta$ | $\alpha$ | $L_x \times L_y \times L_z$ | $N_x \times N_y \times N_z$ | $\Delta x^+$ | $\Delta y^+$ | $\Delta z^+$ |
|---|---|---|---|---|---|---|---|---|---|
| Drag-reducing flow | 150 | 40 | 0.2 | 0.001 | 10 h × 2 h × 4 h | 96 × 128 × 96 | 15.6 | 0.2–4.5 | 6.3 |
| Newtonian | 150 | × | 0 | × | 7.5 h × 2 h × 2.5 h | 128 × 128 × 128 | 8.8 | 0.2–4.5 | 2.9 |

and

$$Nu = \frac{2h^* h}{k} = 2Re_\tau Pr/\Theta_b^+ \quad (6)$$

The drag-reduction rate DR% and heat transfer reduction HTR% are defined as the reduction of friction factor and Nusselt number with respect to the Newtonian fluid at the same mean Reynolds number for the Newtonian fluid and the drag-reducing flow by additives.

## 3. Results

First we concisely compared the results of Newtonian fluid with experimental data and previous numerical results [18] to verify our code. The calculated mean Reynolds number $Re_b = 2\rho U_b h/\mu$ based on the mean velocity and the height of the channel for Newtonian fluid is 4646. The calculated friction coefficient and the ratio of the mean centerline velocity to the bulk mean velocity ($U_c/U_b$) are $8.34 \times 10^{-3}$ and 1.18, respectively. These values agree well with the corresponding values of $8.84 \times 10^{-3}$ and 1.16, which are evaluated by Dean's correlations [19], $c_f = 0.073Re_b^{-0.25}$ and $U_c/U_b = 1.28Re_b^{-0.0116}$, respectively. The calculated Nusselt number is 15.3, which is in good agreement with the value 15.9 evaluated by the correlation of Kays and Crawford $Nu = 0.022Re_b^{0.8}Pr^{0.5}$ [20]. The mean temperature distribution is given in Fig. 2, in which the temperature profile of Kasagi et al. at the same computational parameters is presented for comparison. The agreement between the two temperature profiles is relatively good. The agreements for other quantities between the present results and those of Kasagi et al. [18] are seen in the subsequent figures.

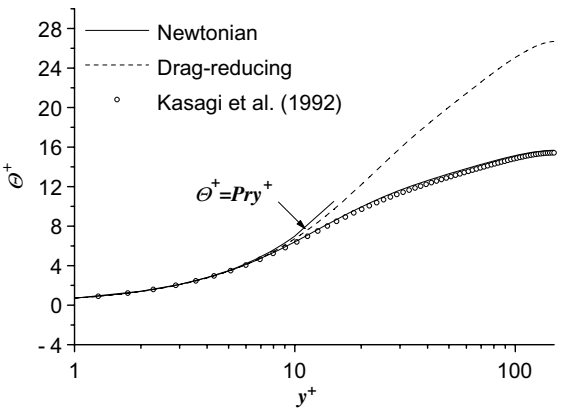


Fig. 2. Mean temperature profiles.

Mean flow variables such as mean Reynolds number, friction factor and Nusselt number are given in Table 2. In Table 2, $c_f^*$ and $Nu^*$ were evaluated by Dean's correlation [19] and Kays and Crawford's correlation [20], respectively, for comparison. As shown in Table 2, the friction factor and Nusselt number of the drag-reducing flow are much smaller than those of the Newtonian fluid, and a drag-reduction rate of 46.8% and heat transfer reduction rate of 54.5% were obtained for the drag-reducing flow. The larger heat transfer rate than drag-reduction rate has been confirmed by experiments [12–14]. The experimental phenomena such as wider buffer layer, reduction of Reynolds shear stress and larger streak spacing between low-speed streaks were reproduced in the simulation (data not shown).

It should be pointed out that we compared the drag-reduction characteristics by use of a Giesekus model with the experimental data and good agreement was obtained [11]. Recently the author's group experimentally studied the characteristics of turbulence transport for momentum and heat [14] but heat transfer was in the developing region. To the author's best knowledge no one has measured the turbulence transport for a fully developed heat transfer of a drag-reducing flow. Thus in this study we did not make a quantitative comparison between the numerical simulation and experimental data. However the major experimental findings in the developing heat transfer regions [14] are reproduced in the numerical simulation as shown in the subsequent figures such as the upshift of mean temperature profile, increase of temperature fluctuations, decrease of wall-normal turbulent heat flux and the decrease of the cross-correlation coefficients between wall normal velocity and temperature.

The dimensionless temperature profiles as a function of $y^+$ are shown in Fig. 2. The mean temperature profiles of the Newtonian fluid and drag-reducing flow collapse to the linear relationship $\Theta^+ = Pry^+$ in the viscous sublayer and the profile of the drag-reducing flow upshifts in the logarithmic layer. Fig. 3 shows that the streamwise velocity fluctuations are appreciably enhanced while the fluctuations of the other two velocity components are dramatically depressed by additives. Fig. 4 shows that the additives activates the temperature fluctuation. The maximum temperature fluctuation intensity

Table 2
Mean flow variables

| | $U_b$ | $U_c$ | $U_c/U_b$ | $Re_b$ | $C_f$ | $C_f^*$ | $Nu$ | $Nu^*$ | DR% | HTR% |
|---|---|---|---|---|---|---|---|---|---|---|
| Drag-reducing flow | 21.5 | 26.6 | 1.24 | 6450 | 0.00433 | 0.00815 | 9.3 | 20.7 | 46.8 | 54.5 |
| Newtonian | 15.5 | 18.3 | 1.18 | 4640 | 0.00834 | 0.00884 | 15.3 | 15.9 | × | × |

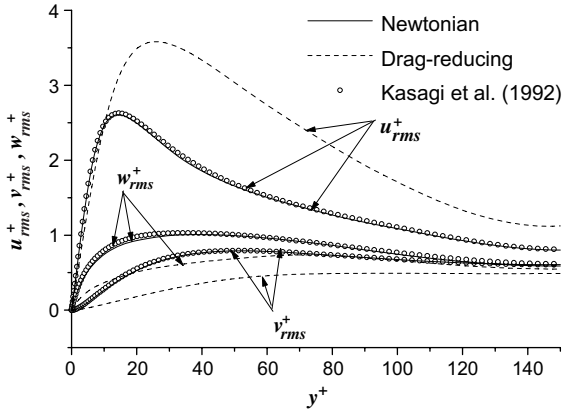


Fig. 3. Velocity fluctuation intensities.

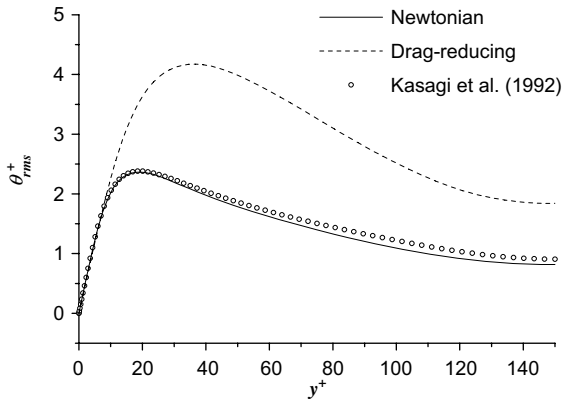


Fig. 4. RMS of temperature fluctuation.

of the drag-reducing flow is 4.2, which is much larger than the value of 2.4 of the Newtonian fluid. The peak temperature fluctuation is located at $y^+ = 35$, which is shifted to the bulk flow region as compared to the peak position $y^+ = 18$ of the Newtonian fluid. Note this value is larger than that of the maximum streamwise velocity fluctuation $y^+ = 28$. Fig. 5 shows that the streamwise turbulent heat flux of the drag-reducing flow is much larger than that of Newtonian flow and the position of its maximum value is shifted toward the bulk flow region. The significant increase of the streamwise heat flux is primarily owing to both the increase of the streamwise velocity fluctuation and the increase of the temperature fluctuation.

Fig. 6(a) and (b) compare velocity-streaks and thermal-streaks at $y^+ = 15$ for the drag-reducing flow. It is seen that the thermal streaky structures closely resemble the velocity streaky structures, and that high-temperature fluids are associated with high-speed streaks and low-temperature fluids are associated with low-speed steaks. The similarity indicates a close correlation between the streamwise velocity component and temperature. In fact, as shown in Fig. 7, the cross-correlation coefficients between $u$ and $\theta$ have large values close to unity. As compared to the Newtonian fluid, $R_{u\theta}$ of the drag-reducing flow increases. The close correlation is another cause for the increase of the streamwise turbulent heat flux. Fig. 6(b) and (c) compare snapshots of the instantaneous temperature fluctuations in the $x$–$z$ plane located at $y^+ = 15$ for drag-reducing flow and Newtonian flow. It is seen that the thermal streaks are more elongated and thermal streak spacing expands by additives.

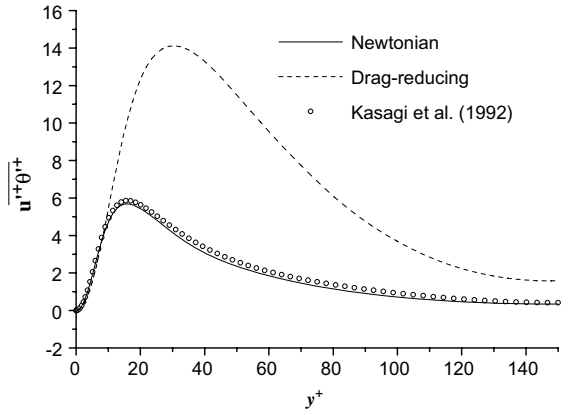


Fig. 5. Streamwise turbulent heat flux.

For the fully developed channel flow between the isoflux walls, the total heat flux can be deduced from the averaged energy equation as follows:

$$q^+_{\text{total}} = 1 - \frac{\int_0^{y^+} U^+ \,\mathrm{d}y^+}{\int_0^{Re_\tau} U^+ \,\mathrm{d}y^+} = \frac{1}{Pr}\frac{\partial \Theta^+}{\partial y^+} - \overline{v'^+\theta'^+} \tag{7}$$

Unlike streamwise turbulent heat flux, the wall-normal turbulent heat flux of drag-reducing flow by additives decreases as compared to Newtonian flow as shown in Fig. 8. The position of its maximum value also shifts to the bulk flow. The strongly suppressed wall-normal velocity fluctuation shown in Fig. 3 is a cause of the reduction of wall-normal heat flux. For the drag-reducing flow, there is an increase of the conductive heat flux to compensate for the decrease of wall-normal heat flux as shown in Fig. 8. This means conduction plays a more important role in heat transportation in the drag-reducing flow. Fig. 7 shows that compared to the Newtonian case, both $R_{uv}$ and $R_{v\theta}$ decrease and the position of their maximum value shifts to the bulk flow. The decreases of $R_{uv}$ and $R_{v\theta}$ indicate that the correlation between the velocity components $u$ and $v$, and that between $v$ and $\theta$ decrease. These decorrelations are believed to be the cause of drag reduction and heat transfer reduction. In addition, for both the Newtonian fluid and drag-reducing flow, the agreement

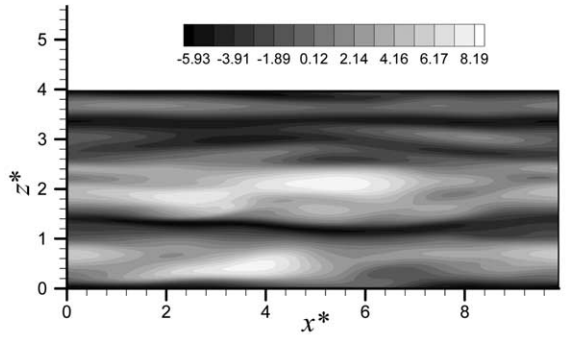


(a) Velocity streaks of viscoelastic flow

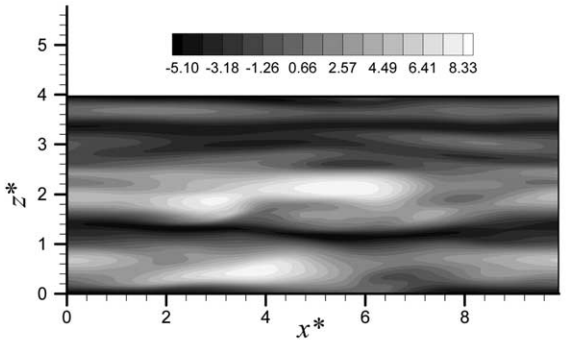


(b) Thermal streaks of viscoelastic flow

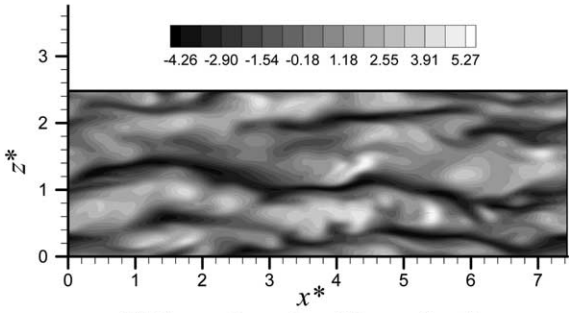


(c) Thermal streaks of Newtonian flow

Fig. 6. Instantaneous speed streaky and thermal streaky patterns the $x$–$z$ plane located at $y^+ = 15$.

between $R_{uv}$ and $R_{v\theta}$ is good. These similarities indicate that the wall-normal turbulent heat flux and Reynolds shear stress are generated by a similar turbulent mechanism for both Newtonian flow and drag-reducing flow by additives.

The nondimensional eddy diffusivities of momentum and heat are shown in Fig. 9. The decrease of both the eddy diffusivities of the drag-reducing flow indicates that less frequent and weaker turbulent transportation occur in the heat and fluid flow process. The turbulent Prandtl number, defined as the ratio between eddy diffusivities for momentum and heat, is shown in Fig. 10. The turbulent Prandtl numbers for both the drag-reducing flow and the Newtonian fluid in the vicinity of the wall approach unity. In the logarithmic region, the turbulent Prandtl numbers of the drag-reducing flow are larger that those of the Newtonian fluid.

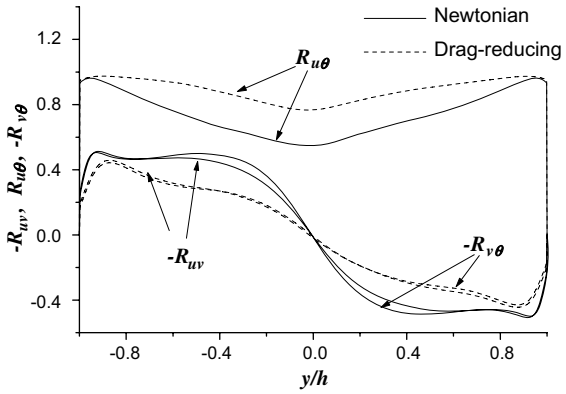


Fig. 7. Cross-correlation coefficients.

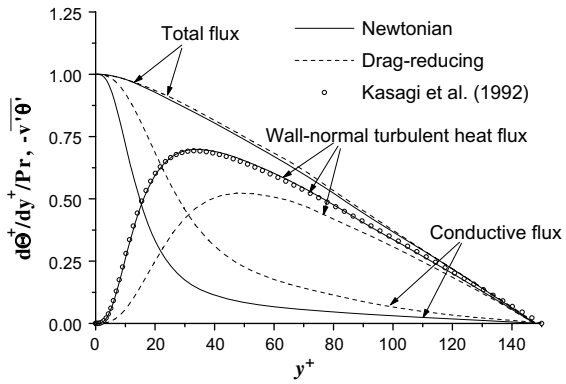


Fig. 8. Budget of heat flux.

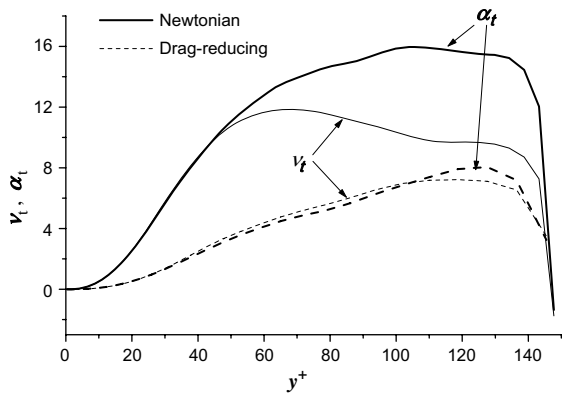


Fig. 9. Eddy diffusivities.

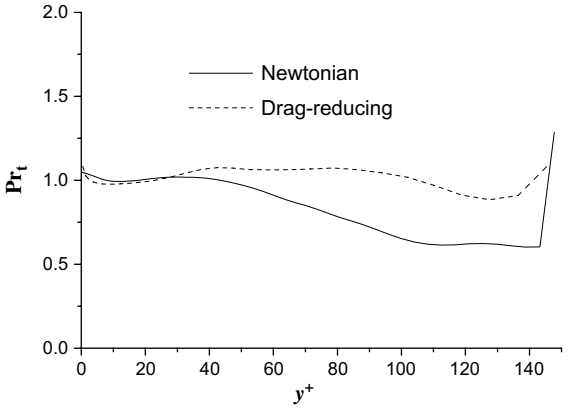


Fig. 10. Turbulent Prandtl number.

The following are the budget equations for streamwise turbulent heat flux $\overline{u'^+\theta'^+}$, wall-normal turbulent heat flux $\overline{v'^+\theta'^+}$, Reynolds normal stress $\overline{u'^+u'^+}$ and Reynolds shear stress $\overline{u'^+v'^+}$, respectively

$$0 = \underbrace{-\overline{u'^+v'^+}\frac{\partial \Theta^+}{\partial y^+}}_{\text{Production}} + \overline{u'^+u'^+}\frac{\partial \langle T\rangle^+}{\partial x^+} \underbrace{-\overline{v'^+\theta'^+}\frac{\partial U^+}{\partial y^+}}_{\text{Production}} - \underbrace{\left(1+\frac{1}{Pr}\right)\overline{\frac{\partial u'^+}{\partial x_i^+}\frac{\partial \theta'^+}{\partial x_i^+}}}_{\text{Dissipation}} - \underbrace{\overline{\theta'^+\frac{\partial p'^+}{\partial x^+}}}_{\text{Temperature pressure–gradient correlation}} - \underbrace{\frac{\partial}{\partial y^+}\left(\overline{u'^+\theta'^+v'^+}\right)}_{\text{Turbulent diffusion}} + \underbrace{\frac{\partial}{\partial x_i^+}\left(\overline{\theta'^+\frac{\partial u'^+}{\partial x_i^+}} + \frac{1}{Pr}\overline{u'^+\frac{\partial \theta'^+}{\partial x_i^+}}\right)}_{\text{Molecular diffusion}} + \underbrace{\frac{2\beta}{We_\tau}\overline{\theta'^+\frac{\partial c'^{+}_{xx_i}}{\partial x_i^+}}}_{\text{Viscoelastic contribution}} \tag{8}$$

$$0 = \underbrace{-\overline{v'^+v'^+}\frac{\partial \Theta^+}{\partial y^+}}_{\text{Production}} + \overline{u'^+v'^+}\frac{\partial \langle T\rangle^+}{\partial x^+} \underbrace{-\left(1+\frac{1}{Pr}\right)\overline{\frac{\partial v'^+}{\partial x_i^+}\frac{\partial \theta'^+}{\partial x_i^+}}}_{\text{Dissipation}} - \underbrace{\overline{\theta'^+\frac{\partial p'^+}{\partial y^+}}}_{\text{Temperature pressure–gradient correlation}} - \underbrace{\frac{\partial}{\partial y^+}\left(\overline{v'^+\theta'^+v'^+}\right)}_{\text{Turbulent diffusion}} + \underbrace{\left[\frac{\partial}{\partial x^+}\left(\overline{\theta'^+\frac{\partial v'^+}{\partial x_i^+}} + \frac{1}{Pr}\overline{v'^+\frac{\partial \theta'^+}{\partial x_i^+}}\right)\right]}_{\text{Molecular diffusion}} + \underbrace{\frac{2\beta}{We_\tau}\overline{\theta'^+\frac{\partial c'^{+}_{x_iy}}{\partial x_i^+}}}_{\text{Viscoelastic contribution}} \tag{9}$$

$$0 = \underbrace{-2\overline{u'^+v'^+}\frac{\partial U^+}{\partial y^+}}_{\text{Production}} \underbrace{-2\overline{\frac{\partial u'^+}{\partial x_i^+}\frac{\partial u'^+}{\partial x_i^+}}}_{\text{Dissipation}} - \underbrace{2\overline{u'^+\frac{\partial p'^+}{\partial x^+}}}_{\text{Velocity pressure–gradient correlation}} - \underbrace{\frac{\partial}{\partial y^+}\left(\overline{u'^+u'^+v'^+}\right)}_{\text{Turbulent diffusion}} + \underbrace{\frac{\partial^2\overline{u'^+u'^+}}{\partial y^2}}_{\text{Molecular diffusion}} + \underbrace{\frac{2\beta}{We_\tau}\overline{u'^+\frac{\partial c'^{+}_{xx_i}}{\partial x_i^+}}}_{\text{Viscoelastic contribution}} \tag{10}$$

$$0 = \underbrace{-\overline{v'^+ + v'^+}\frac{\partial U^+}{\partial y^+}}_{\text{Production}} \underbrace{-2\overline{\frac{\partial u'^+}{\partial x_i^+}\frac{\partial v'^+}{\partial x_i^+}}}_{\text{Dissipation}} \underbrace{-\overline{u'^+\frac{\partial p'^+}{\partial y^+} + v'^+\frac{\partial p'^+}{\partial x^+}}}_{\text{Velocity pressure–gradient correlation}} - \underbrace{\frac{\partial}{\partial y^+}\left(\overline{u'^+v'^+v'^+}\right)}_{\text{Turbulent diffusion}} + \underbrace{\frac{\partial^2\overline{u'^+v'^+}}{\partial y^2}}_{\text{Molecular diffusion}} + \underbrace{\frac{\beta}{We_\tau}\overline{u'^+\frac{\partial c'^{+}_{yx_i}}{\partial x_i^+} + v'^+\frac{\partial c'^{+}_{xx_i}}{\partial x_i^+}}}_{\text{Viscoelastic contribution}} \tag{11}$$

The various terms in the budget of the streamwise turbulent heat flux and wall-normal turbulent heat flux are plotted in Figs. 11 and 12 as a function of dimensionless wall distance $y^+$. As compared to the Newtonian fluid, an additional viscoelastic contribution term is included in the budget of the turbulent heat fluxes. The maximum and minimum values associated with various turbulence quantities of the drag-reducing flow, such as production, display a dramatic decrease. The locations where production attains its maximum value, and where molecular diffusion and turbulent diffusion

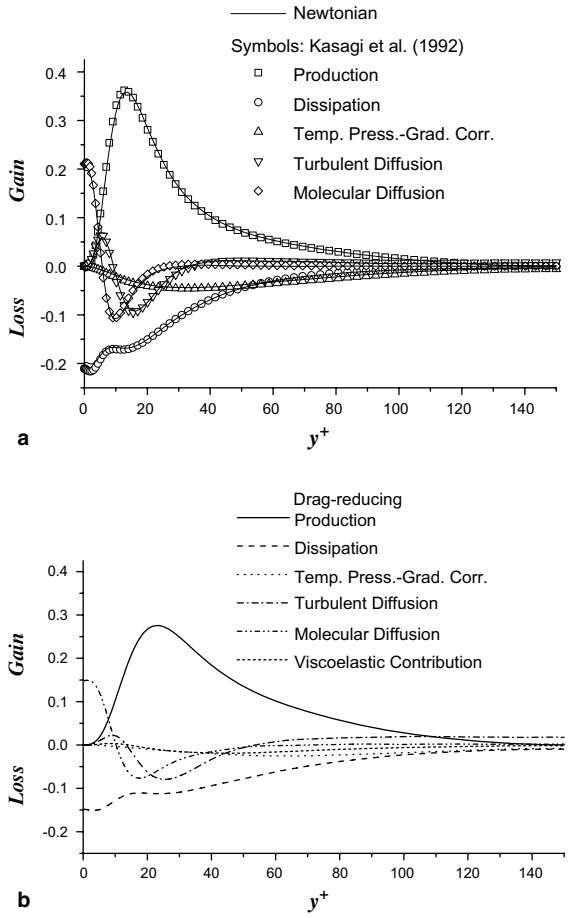


Fig. 11. Budget terms of streamwise turbulent heat flux. (a) Newtonian fluid, (b) drag-reducing flow.

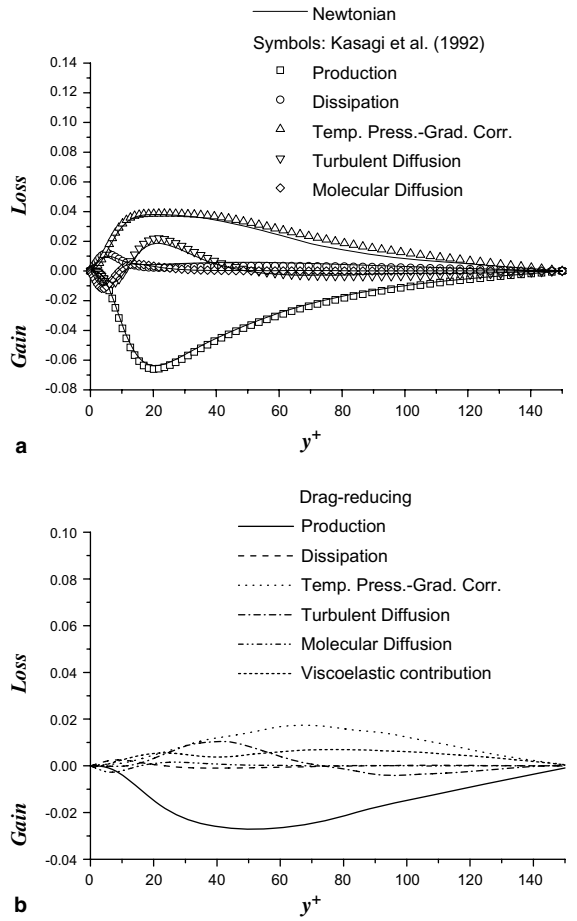


Fig. 12. Budget terms of wall-normal turbulent heat flux. (a) Newtonian fluid, (b) drag-reducing flow.

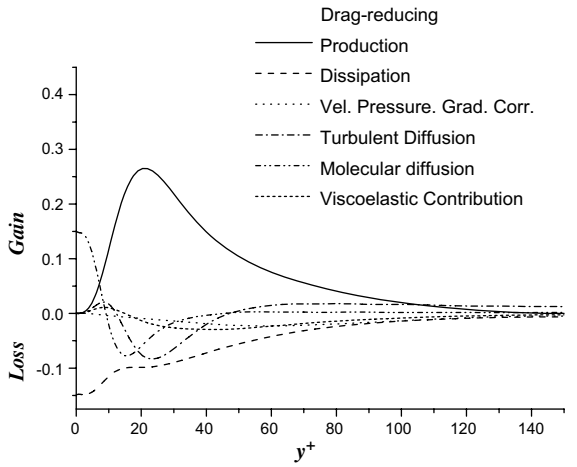


Fig. 13. Budget terms of Reynolds normal stress $\overline{u'^+u'^+}$ of the drag-reducing flow by additives.

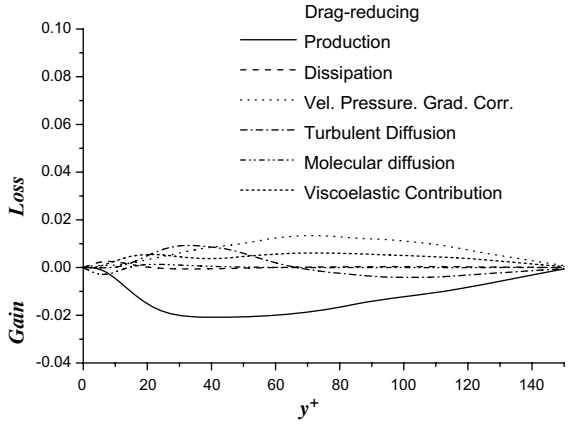


Fig. 14. Budget terms of Reynolds shear stress $\overline{u'^+v'^+}$ of the drag-reducing flow by additives.

reach their minimum values, shift from the wall region to the bulk flow region. These shifts are consistent with the expansion of the buffer layer. Though the additives significantly change the values and distribution of the budget terms, the production, turbulent diffusion, molecular diffusion and other terms show identical trends in variation between Newtonian solution and drag-reducing flow, with the latter varying flatly. In the budget of streamwise turbulent heat flux, the viscoelastic contribution acts as a weak sink term except in the vicinity of the wall, at which it acts as a minute production term. However, in the budget of wall-normal turbulent heat flux, the viscoelastic term is of the same order of magnitude as the other terms (for example, production term) and it acts as a large sink term. There are three peaks (two positive and one negative peaks) for the viscoelastic term in the budget of $\overline{v'^+\theta'^+}$, which are located near the peaks of the molecular diffusion, turbulent diffusion and temperature pressure-gradient correlation. Figs. 13 and 14 show the budget of Reynolds normal stress $\overline{u'^+u'^+}$ and Reynolds shear stress $\overline{u'^+v'^+}$, respectively. Note that the profile of each term in the budget of $\overline{u'^+\theta'^+}$ and $\overline{v'^+\theta'^+}$ is quite similar to the corresponding term in the budget of $\overline{u'^+u'^+}$ and $\overline{u'^+v'^+}$, respectively. These again indicate a high correlation between $u'$ and $\theta'$ as mentioned previously.

The budget equation of the fluctuating temperature variance $k_\theta$, in the fully developed turbulent channel thermal field can be written as

$$0 = \underbrace{\overline{u'^+\theta'^+}\frac{\partial\langle T\rangle^+}{\partial x^+}}_{\text{Production}} - \overline{v'^+\theta'^+}\frac{\partial\Theta^+}{\partial y^+} - \underbrace{\frac{1}{Pr}\left(\overline{\frac{\partial\theta'^+}{\partial x_i^+}\frac{\partial\theta'^+}{\partial x_i^+}}\right)}_{\text{Dissipation}} - \underbrace{\frac{\partial\overline{v'^+\theta'^{+2}}/2}{\partial y^+}}_{\text{Turbulent diffusion}} + \underbrace{\frac{1}{Pr}\frac{\overline{\partial^2\theta'^{+2}}/2}{\partial y^{+2}}}_{\text{Molecular diffusion}} \tag{12}$$

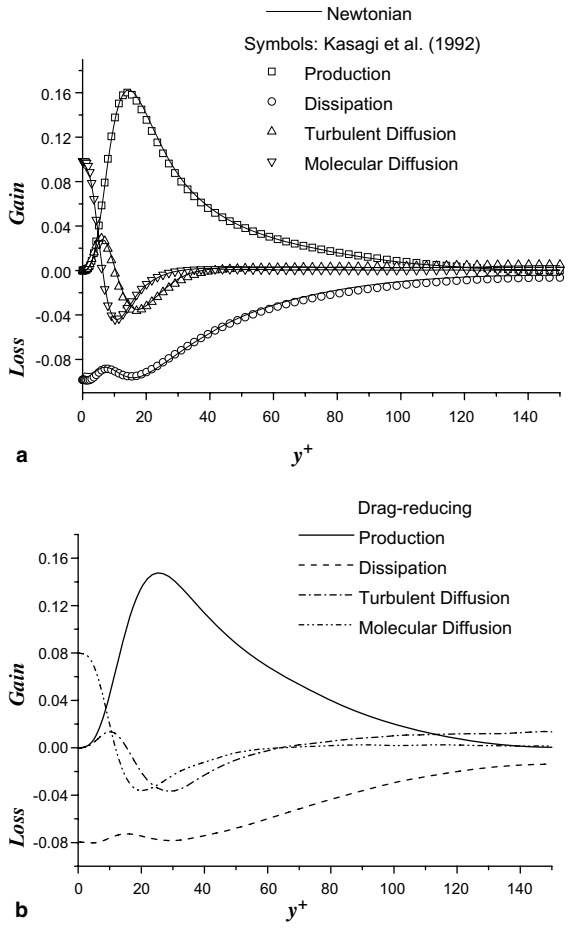


Fig. 15. Budget terms of temperature variance. (a) Newtonian fluid, (b) drag-reducing flow.

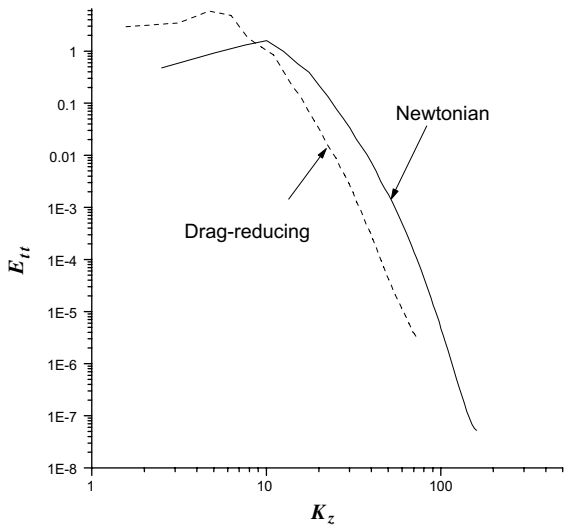


Fig. 16. One-dimensional energy spectrum of the temperature fluctuations vs the spanwise wavenumber at $y^+ = 15$.

The budgets of the temperature variance are shown in Fig. 15. Once again, the position of the peak value shifts toward the bulk flow due to the action of additives. Although the peak values decrease, the magnitudes of the quantities are not depressed in the whole region.

Fig. 16 the one-dimensional energy (Fourier) spectrum of temperature fluctuation at $y^+ = 15$. $E_{tt}$ is one-dimensional energy spectra of temperature fluctuation. $K_z$ is the wave number for the spanwise direction. It is seen the energy contained in low wavenumber modes increase and the peak of the energy spectrum shifts to a higher wavelength in the drag-reducing flow, indicating a larger thermal streak spacing in the drag-reducing flow. This also indicates the large scale temperature fluctuations are created but small scales of temperature fluctuations are dampened by additives.

## 4. Conclusions

A DNS on the turbulent heat transfer in the channel flow of a drag-reducing flow was carried out. The computational parameters were $Re_\tau = 150$, $We_\tau = 40$, $\alpha = 0.001$ and $\beta = 0.2$ for the Giesekus model employed. The following conclusions can be drawn:

(1) A drag-reduction rate of 46.8% and heat transfer reduction rate of 54.5% were obtained.
(2) The intensity of temperature fluctuation increases appreciably by additives.
(3) As compared to Newtonian flow, the streamwise turbulent heat flux of the drag-reducing flow becomes larger and the position of its peak value shifts toward the bulk flow region. The increase of the streamwise turbulent heat flux is due to the enhancements of the streamwise velocity fluctuation and temperature fluctuation, and also due to the increase of the correlation between the streamwise velocity fluctuation and temperature fluctuation.
(4) The wall-normal turbulent heat flux of the drag-reducing flow decreases, which is due to the strongly suppressed wall-normal velocity fluctuation intensity and the lower correlation between the wall-normal velocity fluctuation and the temperature fluctuation.
(5) The additives decreases the magnitude of the budget terms in the streamwise and wall-normal turbulent heat fluxes, and the total contribution of the additives acts as a weak sink term except in the vicinity of the wall in the budget of the streamwise turbulent heat flux and as a large sink term in the budget of the wall-normal heat flux.
(6) As compared to the Newtonian fluid, the thermal streak spacing of the drag-reducing flow by additives expands.

## Acknowledgements

We are grateful to Prof. T. Kajishima at Osaka University and Dr. K. Fukagata at Tokyo University for their valuable discussions on DNS. The authors also thank their colleagues at AIST for their help during this study. This research was supported by the Ministry of Education, Culture, Sports, Science and Technology through the project, "Smart Control of Turbulence: A Millennium Challenge for Innovative Thermal and Fluid Systems" of Japan.

## References

[1] B.A. Toms, Some observations on the flow of linear polymer solutions through straight tubes at large Reynolds numbers, in: Proc. 1st Int. Congress on Rheology, North Holland, Amsterdam, 1948, pp. 135–141.
[2] P. Orlandi, A tentative approach to the direct simulation of drag reduction by polymers, J. Non-Newtonian Fluid Mech. 60 (1995) 277–301.
[3] J.M.J. DenToonder, M.A. Hulsen, G.D.C. Kuiken, F.T.M. Nieuwstadt, Drag reduction by polymer additives in a turbulent pipe flow: numerical and laboratory experiments, J. Fluid Mech. 337 (1997) 193–231.
[4] R. Sureshkumar, A.N. Beris, R.A. Handler, Direct numerical simulation of turbulent channel flow of a polymer solution, Phys. Fluids 9 (1997) 743–755.
[5] C.D. Dimitropoulos, R. Sureshkumar, A.N. Beris, Direct numerical simulation of viscoelastic turbulent channel flow exhibiting drag reduction: effect of the variation of rheological parameters, J. Non-Newtonian Fluid Mech. 79 (1998) 433–468.
[6] T. Min, J.Y. Yoo, H. Choi, D.D. Joseph, A role of elastic energy in turbulent drag reduction by polymer additives, in: Proc. 2nd International Symposium on Turbulence and Shear Flow Phenomena, KTH, Stockholm, vol. 3, 2001, pp. 35–50.
[7] E. De Angelis, C.M. Casciola, R. Piva, DNS of wall turbulence: dilute polymers and self-sustaining mechanisms, Comput. Fluids 31 (2002) 495–507.
[8] H. Suzuki, K. Ishihara, H. Usui, Numerical study on a drag-reducing flow with surfactant additives, in: Proc. 3rd Pacific Rim Conference on Rheology, 2001.
[9] B. Yu, Y. Kawaguchi, Direct numerical simulation of the viscoelastic drag-reducing flow: a faithful finite-difference method, J. Non-Newtonian Fluid Mech. 116 (2004) 431–466.
[10] B. Yu, Y. Kawaguchi, Effect of Weissenberg number on the flow structure: DNS study of drag-reducing flow with surfactant additives, Int. J. Heat Fluid Flow 24 (2003) 491–499.
[11] B. Yu, F.Ch. Li, Y. Kawaguchi, Numerical and experimental investigation on turbulence characteristics in a drag-reducing flow with surfactant additives, Int. J. Heat Fluid Flow 25 (6) (2004) 961–974.
[12] F.Ch. Li, Y. Kawaguchi, K. Hishida, The influence of a drag-reducing surfactant on turbulent velocity and temperature field of a 2D channel flow, Exp. Fluids 36 (1) (2004) 131–140.
[13] F. Ch. Li, Y. Kawaguchi, T. Segawa, K. Hishida, Influence of drag-reducing surfactant additives on vortex structures and turbulent events in a channel flow, 2004 ASME Heat Transfer/Fluids Engineering Summer Conference, July 11–15, Charlotte, NC, USA.
[14] F.Ch. Li, Y. Kawaguchi, K. Hishida, Investigation on the characteristics of turbulent transport for momentum and heat in a drag-reducing surfactant solution flow, Phys. Fluids 16 (9) (2004) 3281–3295.
[15] H. Tennekes, J.L. Lumley, A First Course in Turbulence, MIT Press, Cambridge, MA, 1972.
[16] R. Friedrich, T.J. Huttl, M. Manhart, C. Wagner, Direct numerical simulation of incompressible turbulent flows, Comput. Fluids 30 (2001) 555–579.
[17] D.M. Lu, G. Hetsron, Direct numerical simulation of a turbulent open channel flow with passive heat transfer, Int. J. Heat Mass Transfer 38 (1995) 3241–3251.
[18] N. Kasagi, Y. Tomita, A. Kuroda, Direct numerical simulation of passive scalar field in a turbulent channel flow, Trans. ASME, J. Heat Transfer 114 (1992) 589–606.
[19] R.B. Dean, Reynolds number dependence of skin friction and other bulk flow variables in two-dimensional rectangular duct flow, Trans. ASME, J. Fluids Eng. 100 (1978) 215–223.
[20] W.M. Kays, M.E. Crawford, Convective Heat and Mass Transfer, second ed., McGraw-Hill, New York, 1980.